Acta Crystallographica Section B
Structural Science
ISSN 0108-7681

Second-degree twinning and dynamic disorder in the crystal structure of deca-dodecasil 3*R*

Vratislav Langer,[a] Ľubomír Smrčok,[b]* Daniel Tunega[c,d] and Gernot Wirnsberger[e]

[a]Department of Chemical and Biological Engineering, Division of Materials and Surface Chemistry, Subdivision of Inorganic Environmental Chemistry, Chalmers University of Technology, SE-412 96 Göteborg, Sweden, [b]Institute of Inorganic Chemistry, Slovak Academy of Sciences, Dúbravská cesta 9, SK-845 36 Bratislava, Slovakia, [c]Austrian Research Centres, A-2444 Seibersdorf, Austria, [d]Institute for Theoretical Chemistry, University of Vienna, Währingerstrasse 17, A-1090 Vienna, Austria, and [e]Mühlgasse 5, A-8700 Leoben, Austria

Correspondence e-mail: uachsmrk@savba.sk

Received 9 May 2005
Accepted 21 August 2005

The structure of deca-dodecasil 3*R* (DD-3*R*), $Si_{120}O_{240}$, a very well suited material for the synthesis of inorganic/organic composites structured on a nanometer level, has been investigated in detail. So far, a highly complicated twinning has hampered its structure description at a desirable level of accuracy. This twinning has now been resolved and a new structure determination is presented. Structure refinement in the $R\bar{3}$ space group revealed a large, unusually shaped atomic displacement ellipsoid for oxygen-bridging units (tetrahedra), bridging Si—O bonds shorter than expected and the linear Si—O—Si′ bond angle dictated by special positions at a threefold axis. A structure model based on a statistically disordered bridging O atom improved the accuracy of the Si—O bonds of interest, but provided unacceptable O—O contacts. To solve this dilemma, *ab initio* NVT molecular dynamics calculations were performed to study the possible configurations. Wavelet analysis of the time variations of selected Si—O distances pointed to a synchronous shift of the whole building units (tetrahedra). Low-frequency features of the calculated phonon density of states agree well with the published INS (inelastic neutron scattering) spectra of several silica polymorphs, indicating that the nature of the disorder in DD-3*R* is dynamic rather than static.

1. Introduction

Porosils are an intriguing class of porous materials, exclusively composed of SiO_2, with voids of up to *ca* 20 Å and hence represent microporous modifications of silica. Generally these SiO_2 modifications can be synthesized under hydrothermal conditions using organic and/or inorganic templates and a source of silica. After synthesis the templates can be removed, leaving behind fully connected SiO_2 frameworks that constitute highly porous solid-state materials with accessible pores or channels. Such structures with pores and channels are well suited hosts for a designed arrangement of inorganic guest components, which can be inserted into the voids whereby the alignment of the guest molecules and their intermolecular interaction can be tuned.

Among porosils used for the insertion of inorganic molecules (Wirnsberger *et al.*, 1997, 1999), deca-dodecasil 3*R* (DD-3*R*) has attracted special interest because it possesses cages and it can be used as an inert but well ordered solid-state matrix for inorganic molecules. When included within the DD-3*R* cages, inorganic molecules are perfectly isolated from each other and can be probed by spectroscopy (Ermoshin *et al.*, 1999, 2001). As opposed to Ar, Xe or the other inert solid matrices usually employed in spectroscopic matrix isolation studies, DD-3*R* represents a well ordered crystalline matrix around the investigated molecules, which opens the possibility

of studying weak host–guest interactions in detail, as well as the influence of the matrix.

One prerequisite for such advanced studies, however, is a good knowledge of the host structure. Deca-dodecasil 3*R* with 1-aminoadamantane as a guest molecule was first prepared and characterized by X-ray diffraction (Gies, 1986), TEM (Gies & Czank, 1986) and ^{29}Si MAS NMR (Almazeestraten *et al.*, 1987). The separation of permanent gases using the DD-3*R* and its adsorption properties were first studied by den Exter and coworkers (den Exter *et al.*, 1994, 1997). Unfortunately, the crystal structure determination of DD-3*R* containing 1-aminoadamantane by Gies (1986) suffered from twinning of the DD-3*R* crystals. Even though the twinning was correctly recognized by Gies, it was not handled properly and the best fit between the model and the observed data (with overlapping diffracted peaks omitted) was no better than $R = 0.191$. As DD-3*R* is a very interesting crystalline host for matrix isolation studies of isolated molecules up to temperatures at which they start to desorb, we investigated the structure of DD-3*R* in detail.

2. Synthesis

Crystals of DD-3*R* were prepared by a method first reported by van de Goor (1995). In a typical synthesis, 3.3 mmol of 1-aminoadamantane were suspended in 10 ml of deionized H_2O. After stirring for 15 min, 0.822 g of NH_4F were added and the resulting mixture was stirred for a further 10 min. In the next step 0.13 ml of 40 wt.-% HF were added to the homogenous suspension. Finally, 1.33 g of SiO_2 were mixed into the suspension (10 min after addition the of HF). The highly viscous gel was homogenized by stirring for around 1 h and thereafter filled into a teflon-lined steel autoclave with a free volume of 10 ml (degree of filling = 80%). The closed autoclave was placed in a forced air oven at 433 K for 3 weeks to allow crystallization. After the reaction had been completed, the autoclave was allowed to cool down to room temperature and the product was filtered off. In order to remove residual amorphous SiO_2 the product was washed with 100 ml of NaOH, followed by 200 ml of H_2O. Using this method, 0.833 g of platy hexagonal crystals were obtained.

Calcination (oxidative removal of the organic guest molecules) was performed by heating crystals from room temperature to 1123 K within 10 h, holding the crystals at this temperature for 4 h and finally cooling down the crystals to room temperature within 24 h. After their calcination, the crystals were colourless and had lost weight corresponding to an initial composition of 120 SiO_2:6.00 $C_{10}H_{17}N$ (the composition of the as-synthesized material was confirmed by TGA).

3. Structure determination

The data were empirically corrected for absorption and other effects using *SADABS* (Sheldrick, 2001), based on the method of Blessing (1995) using the apparent $\bar{3}m1$ Laue symmetry. $R_{\rm int}$ for 44 259 diffractions [$I > 10\sigma(I)$] dropped from 0.0485 to 0.0379. When the resulting diffraction file was inspected using *XPREP* (Siemens, 1995), the statistics revealed a tendency to systematic extinction for a rhombohedral cell, but with many exceptions. Although the mean value of $|E^2 - 1| = 0.739$ [expected value is 0.968 for centrosymmetric and 0.736 for non-centrosymmetric space groups (Wilson, 1985)] indicates well the non-centrosymmetric structure (typical behaviour for twinned crystals according to Herbst-Irmer & Sheldrick, 1998), the space group $R\bar{3}$ was chosen. All reflections fulfilling the systematic extinctions imposed by the *R* cell were merged at the point group $\bar{3}$, giving $R_{\rm int} = 0.0307$ and 3621 symmetrically independent reflections.

The structure was solved using direct methods with the *SHELXTL* package (Bruker, 2001). A preliminary refinement was not very successful giving $R = 0.304$ in an isotropic approximation. We first tried a binary twin by merohedry, twin law $2_{[110]}$, dichromatic twin point group $\bar{3}2'/m'1$. With this merohedral twinning introduced into the refinement (transformation $010/100/00\bar{1}$) it behaved much better and $R = 0.098$ was obtained, still in isotropic approximation. Unfortunately, a switch from isotropic to anisotropic approximation did not result in any significant improvement and the *R* dropped to only 0.093.

Bearing in mind the tendency towards the rhombohedral lattice recognized during the initial stage, another kind of binary twinning by reticular merohedry, twin index 3, dichromatic twin point group $6'$, was attempted instead (transformation $\bar{1}00/0\bar{1}0/001$). The *R* value changed from 0.304 to 0.275 (isotropic approximation), *i.e.* worse than when merohedral twinning only was considered, but better than without the inclusion of any twinning. It was then obvious that we had to deal with a combined twinning by merohedry and reticular merohedry, thus having four individuals contributing to the final diffraction pattern. This second-degree twin is characterized (for nomenclature, see Nespolo, 2004) by the quadrichromatic twin point group

$$\left(\frac{6^{(2)}}{m^{(2)}}\frac{2^{(2)}}{m^{(2)}}\frac{2^{(2)}}{m^{(2)}}\right)^{(4)}.$$

A similar case has been described by Hatop *et al.* (2001) and in more detail by Herbst-Irmer & Sheldrick (2002). As the *SHELXTL* program (Bruker, 2001) is unable to handle two types of twinning simultaneously (with the exception of inversion twinning), the diffraction *.hkl* file had to be edited and the HKLF 5 together with MERG 0 command was used.[1] A Fortran program has been written to add to diffractions *hkl* (domain one): the diffraction $-h,-k,l$ if $h - k + l$ is a multiple of 3 (domain two), the diffraction $-k,-h,l$ if both $h - k - l$ and $-h + k + l$ are multiples of 3 (domain three) and the diffraction *khl* if $-k + h + l$ is a multiple of 3 (domain four). Three BASF parameters were also introduced to describe the portion of the four domains (the first domain is a complement to the sum of the other three). This resulted in an *R* value of 0.0244 which is quite acceptable in an anisotropic approximation; all the other indicators and the arrangement of the

[1] More details on these commands can be found in the *SHELXTL* Reference Manual.

Table 1
Experimental details.

Crystal data	
Chemical formula	$O_{120}Si_{60}$
M_r	3605.40
Cell setting, space group	Trigonal, $R\bar{3}$
a, c (Å)	13.7761 (1), 41.5456 (6)
V (Å^3)	6828.23 (12)
Z	2
D_x (Mg m^{-3})	1.754
Radiation type	Mo $K\alpha$
No. of reflections for cell parameters	7657
θ range (°)	2.6–28.3
μ (mm^{-1})	0.66
Temperature (K)	183 (2)
Crystal form, colour	Hexagonal plate, colourless
Crystal size (mm)	0.26 × 0.22 × 0.08
Data collection	
Diffractometer	CCD area detector
Data collection method	ω scans
Absorption correction	Multi-scan (based on symmetry-related measurements)
T_{min}	0.880
T_{max}	0.949
No. of measured, independent and observed reflections	44 259, 3622, 3556
Criterion for observed reflections	$I > 2\sigma(I)$
R_{int}	0.031
θ_{max} (°)	28.3
Range of h, k, l	$-18 \Rightarrow h \Rightarrow 18$ $-18 \Rightarrow k \Rightarrow 18$ $0 \Rightarrow l \Rightarrow 54$
Refinement	
Refinement on	F^2
$R[F^2 > 2\sigma(F^2)]$, $wR(F^2)$, S	0.024, 0.082, 0.95
No. of reflections	3622
No. of parameters	184
Weighting scheme	$w = 1/[\sigma^2(F_o^2) + (0.0757P)^2 + 2.4398P]$, where $P = (F_o^2 + 2F_c^2)/3$
$(\Delta/\sigma)_{max}$	0.001
$\Delta\rho_{max}$, $\Delta\rho_{min}$ (e Å^{-3})	1.12, −0.34

Computer programs used: *SMART*, *SAINT* (Siemens, 1995), *SADABS* (Sheldrick, 2001), *SHELXTL* (Bruker, 2001), *DIAMOND* (Brandenburg, 2005).

atoms showed the structure was correctly solved. The domain fractions refined to: 0.366 (1), 0.131 (1), 0.365 (1) and 0.137 (1) for domains one to four, respectively.

The crystal data, data collection details and structure refinement parameters are presented in Table 1.[2] The atomic coordinates have been deposited. An *ORTEP*-like drawing is given in Fig. 1 and a projection of the structure along the *a* axis is shown in Fig. 2. The essential bond lengths are summarized in Table 2.

4. Results and discussion

Despite the generally very good agreement between the interatomic distances and angles with those that were expected, the analysis of the structure revealed a disc-like atomic displacement ellipsoid of O2. This was reflected by a rather large U_{eq} value, shorter than the Si1—O2 and Si2—O2 bonds expected, and the linear Si1—O2—Si2 group dictated by the atom being located on a threefold axis.

Unacceptably large temperature parameters of O atoms and/or linear Si—O—Si groups have previously intrigued several authors refining the crystal structures of compounds with the chemical composition SiO_2. For instance, in his refinement of the high-cristobalite structure Peacor (1973) found that placing the Si and O atoms at the special positions of the $Fd\bar{3}m$ space group led to a Debye–Waller factor B(O) three times larger than B(Si). A remedy to this problem was a trial positioning of the O atom to the lower-symmetry positions. After a series of refinements the best results were obtained with oxygen moved from the 16(*c*) to the 96(*h*) position: d(Si—O) ≃ 1.61 Å, O—Si—O ≃ 109°, Si—O—Si ≃ 148° and B(Si) ≃ B(O). These results were later corroborated by Schmahl *et al.* (1992), who used time-of-flight neutron powder diffraction data.

Previous refinements of the crystal structure of two polytypes of dodecasil, 1*H* (Miehe *et al.*, 1993) and 3*C* (Könnecke *et al.*, 1992), have also suffered from problems with the large temperature parameters of O atoms and linear Si—O—Si

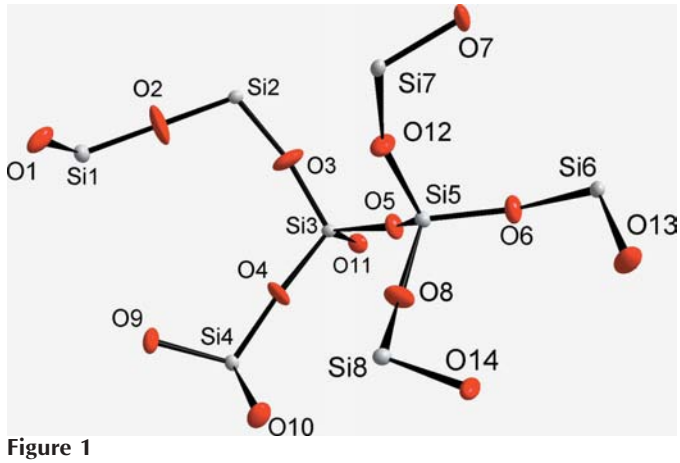

Figure 1
Atomic labeling scheme for the atoms of the title compound. The ellipsoids are drawn at the 50% probability level.

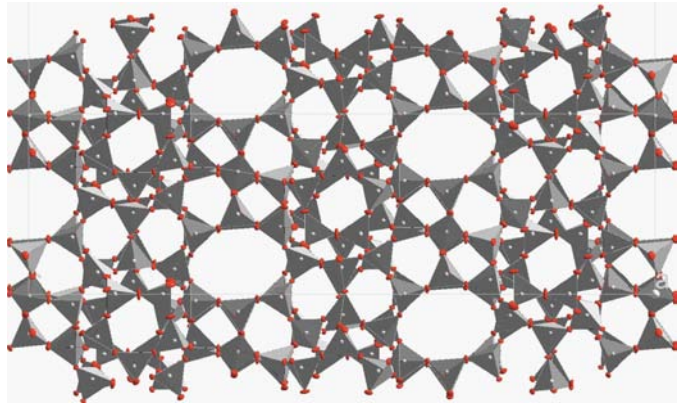

Figure 2
Polyhedral presentation of the structure of DD-3*R*.

[2] Supplementary data for this paper are available from the IUCr electronic archives (Reference: LC5031). Services for accessing these data are described at the back of the journal.

Table 2
Selected interatomic distances (Å) in SiO_4 tetrahedra.

The average O—Si—O′ bond angles in individual tetrahedra are 109.5, 109.5, 109.7, 109.5, 109.3, 110.0, 109 and 109.4°, respectively.

Si1—O2	1.589 (3)	Si5—O8	1.603 (2)
Si1—O1	1.611 (2)	Si5—O5	1.604 (2)
Si1—O1^{i}	1.611 (3)	Si5—O6	1.608 (2)
Si1—O1^{ii}	1.611 (2)	Si5—O12	1.610 (2)
Si2—O2	1.577 (3)	Si6—O13	1.602 (2)
Si2—O3	1.594 (2)	Si6—O6	1.602 (2)
Si2—O3^{ii}	1.594 (3)	Si6—O13^{iii}	1.605 (3)
Si2—O3^{i}	1.594 (2)	Si6—O7	1.614 (2)
Si3—O3	1.599 (2)	Si7—O11^{iv}	1.599 (2)
Si3—O11	1.605 (2)	Si7—O12^{v}	1.601 (2)
Si3—O5	1.605 (2)	Si7—O14^{iii}	1.610 (2)
Si3—O4	1.607 (2)	Si7—O7	1.611 (2)
Si4—O10	1.600 (2)	Si8—O9^{vi}	1.605 (2)
Si4—O4	1.602 (2)	Si8—O1^{vi}	1.606 (2)
Si4—O10^{vi}	1.605 (3)	Si8—O8	1.607 (2)
Si4—O9	1.607 (2)	Si8—O14	1.608 (2)

Symmetry codes: (i) $-y, x-y, z$; (ii) $-x+y, -x, z$; (iii) $-\frac{2}{3}+y, -\frac{1}{3}-x+y, \frac{2}{3}-z$; (iv) $\frac{1}{3}-x, \frac{2}{3}-y, \frac{2}{3}-z$; (v) $\frac{1}{3}+x-y, \frac{2}{3}+x, \frac{2}{3}-z$; (vi) $-\frac{1}{3}+y, \frac{1}{3}-x+y, \frac{1}{3}-z$.

groups. To remove the residual electron density concentrated around the O-atom sites placed in the special positions of the space group *P*6/*mmm* (1*H* polytype), the O atoms had to be split and the refinement supported by restraints. As a result, the mean U_{eq} value decreased and the Si—O—Si angles were within 147–165°. In the 3*C* case, however, the splitting of the O atoms led to only a small decrease in the *R* factor, but 'the effects in the difference Fourier syntheses disappeared'. After a constrained refinement was finished, the mean Si—O—Si angle changed from *ca* 176 to 164°, the maximum values being conspicuous at 180 and 176°, respectively. Since these two refinements were supported by restraints, they do not provide a good benchmark for the analysis of Si—O bond distances and angles. On the contrary, in the refinement of the 3*C* polytype with tetrahydrofuran as a guest molecule (Knorr & Depmeier, 1997), no residual electron densities around the framework O atoms were found. However, one short Si—O distance of 1.567 (4) Å was obtained and even though the mean value of the bridging Si—O—Si angles was 164°, the angles of 172, 175 and 176° were formed.

The fact that the neutron powder diffraction pattern of β-cristobalite contained diffuse scattering in addition to Bragg peaks motivated the total neutron scattering study of both α- and β-cristobalite (Dove, Keen *et al.*, 1997). The most important results of this study are that the local structure of β-cristobalite is fully compatible with the existence of ideal SiO_4 tetrahedra. Second, whilst the medium-range structure of β-cristobalite is *more* ordered than that of silica glass, it is *less* ordered than that of α-cristobalite. Later, Tucker *et al.* (2001) extended this work by applying reverse Monte Carlo modelling. They showed that '... disorder in β-cristobalite involves rotations and displacements of rigid SiO_4 tetrahedra consistent with the prediction of the rigid-unit model (RUM)'. O atoms in β-cristobalite were also found to be distributed continuously rather than in specific crystallographic sites.

In contrast, the existence of linear Si—O—Si groups in the crystal structures of various silicates and silicon dioxide polymorphs was advocated by Baur (1977, 1980). Baur summarized several reliably determined structures where the linear Si—O—Si groups were unambiguously recognized. In his works it was stressed that in those structures the bridging O atoms involved in the linear Si—O—Si bonds were not only placed in the special positions dictated by a respective space group. Moreover, these O atoms were not characterized by any unusual anisotropic temperature parameters.

To solve some ambiguities about the *true* structure of SiO_2 polymorphs some computational approaches were also attempted. Gambhir *et al.* (1999) – performing the molecular dynamics simulation (MD) of cristobalite and quartz – found a remarkable discrepancy between the ways in which the O atoms were placed in the respective structures. While in cristobalite the oxygen positions were best described by an annulus centred on the midpoint between two neighbouring Si atoms (*cf.* DD-1*H*, DD-3*C*, high cristobalite), in quartz only well localized O atoms were indicated. It must be noted, however, that all these simulations were based on the concept of stiff SiO_4 tetrahedra.

Taking into account the variability of the approaches and the results summarized above, a refinement with O2 statistically disordered about the threefold axis was attempted. Owing to the strong correlations an isotropic approximation of O2 was applied. The U_{iso} value for O2 dropped to a very acceptable value of 0.0156 (11) Å^2, but the tetrahedra around Si1 and Si2 were distorted. Considering the results from both refinements the crucial problem was which was most unlikely, a Si—O—Si bridging angle equal to 180° or a distorted SiO_4 tetrahedron? The solution with O2 on the threefold axis gave a shorter than expected Si2—O2 distance (1.576 Å), a linear Si—O—Si angle and rather uniform O—O contact distances (2.60–2.64 Å). On the other hand, refinement with O2 in a general position resulted in all the Si—O distances being very close to the expected value of 1.61 Å and the bridging angle decreased to 160 (3)°. However, the improvement was paid by rather atypical O—O contact distances (2.50, 2.77 Å) and O—Si—O bond angles within the tetrahedra around Si1 and/or Si2 (*ca* 101 and 119°). In other words, the first case gave the barely acceptable shortening of the very strong and stiff polar covalent Si—O bonds, while the second case increased the O—O repulsion due to shorter non-bonding contacts.

5. Computational study

As the time- and volume-averaged structure analyses did not provide a clear picture of the structure of the DD-3*R* polytype, *ab initio* geometry optimizations were attempted for four working structural models. The calculations were performed using the Vienna *ab initio* simulation package (*VASP*; Kresse & Hafner, 1993; Kresse & Furthmüller, 1996) proposed for periodic systems. In this program the theoretical base is density functional theory. The exchange-correlation functional is expressed in the localized density approximation (LDA) according to Perdew & Zunger (1981), together with the

Table 3
Cell volumes and calculated total total energies of four structural models.

Model	V (Å^3)	E (eV)
0.9V	2045.307	−950.903
1.0V	2276.023	−955.104
1.0V (dev)	2276.023	−955.107
1.1V	2510.307	−954.181

generalized gradient approximation (GGA) according to Perdew & Wang (1992). Plane waves form a basis set and calculations are performed using the projector-augmented wave (PAW) method (Blöchl, 1994; Kresse & Joubert, 1999) and atomic pseudo-potentials (Kresse & Hafner, 1994). An optional energy cutoff controls the size of the basis set and thus also the accuracy of the calculation. In our case the energy cutoff of 500 eV was used, *i.e.* a very extended basis set and highly accurate calculations. Since the computational unit cells were sufficiently large, the Brillouin-zone sampling was restricted to the Γ point. The positions of all the atoms in all the models were optimized by applying the conjugate-gradient algorithm using the following convergence criteria: 10^{-5} eV for the electronic energy, 0.001 Å for the r.m.s. atomic displacement and 0.05 eV Å^{-1} for the r.m.s. residual force. The computational cell was a primitive rhombohedral unit cell (a = 15.970 Å, α = 51.102°) in order to reduce the number of optimized atoms to an acceptable 40 Si + 80 O. No symmetry restrictions were applied during the geometry optimization, *i.e.* the calculations were performed in the $P1$ space group. In the course of the optimizations the cell parameters and the cell shape were kept fixed.

In the basic model the initial atomic coordinates were transformed from the coordinates obtained in the refinement, with Si1—O2—Si2 on a threefold axis. Two additional models were derived from the basic model by applying an isostatic compression or expansion of *ca* 10% of the volume of the basic cell. The unit-cell vectors decreased to 15.4 Å in the case of the compression and increased to 16.5 Å in the case of the expansion. The rationale behind those two models was to check whether or not a smaller lattice parameter could force the Si1—O2—Si2 angle to decrease or if a larger cell parameter could give the computational procedure a chance to 'expand' the structure and then relax it to a new minimum with the Si1—O2—Si2 angle < 180°. The fourth model was derived from the basic model by just moving the O2 atom from the Si1—O2—Si2 line to form a new bond angle of 160°.

Relaxation of the basic model led to Si—O distances ranging from 1.597 to 1.622 Å (mean value 1.622 Å), tetrahedral O—Si—O angles distributed around 109° and Si—O—Si angles around the preferred 145°, but the closely monitored Si1—O2—Si2 bond angle remained at *ca* 180°. Similarly, relaxation of the model with the Si1—O2—Si2 angle set to the starting value of 160° ended with the Si1—O2—Si2 angle very close to linearity; the actual value being 175°. While the basic model and the model with O2 shifted from the Si—O—Si line represented the most energetically stable configurations, both compression and expansion led to the remarkable increase of the total electronic energy (Table 3), without having any impact on the angle of the Si—O—Si bridge, which remained at *ca* 180°. The values of the bridging angles near 180° were also preserved in the LDA/GGA calculation of various silica polytypes with less complicated crystal structures (Demuth *et al.*, 1999). Whereas the compression had a negligible effect on the Si—O bond lengths, the volume expansion led to final Si—O bonds being longer by *ca* 0.02 Å compared with the basic model. To summarize, a 'static' picture of the structure obtained from the *ab initio* structural relaxations confirms the existence of a DD-3R structure with the Si—O—Si bridge angle equal to 180°.

As there was a risk that the relaxations could have been entrapped in local minima, molecular dynamics calculations (MD) were carried out in order to inspect the possible configurations. Owing to the number of atoms per unit cell, the type of basis set and overall computational demands, the computational cell was the same as in the static relaxations. The finite-temperature simulations of the dynamical properties were carried out at 300 K and a canonical ensemble with a Nosé thermostat (Nosé, 1984) was used. The Verlet velocity algorithm (Ferrario & Ryckaert, 1985) with

(i) a time step Δt = 1 fs (fast sampling) and simulation time of 4 ps and

(ii) Δt = 4 fs (slow sampling) and simulation time of 20 ps was used.

Compared with 'static' relaxations, molecular dynamics simulations were performed with a somewhat lower accuracy, limited by the use of a plane-wave cutoff energy of 300 eV.

An inspection of the results from the run with the fast sampling (i) revealed the flatness of the energy surface and the vast majority of configurations showed a total energy within the interval not wider than *ca* 0.2% of the average total energy. A statistical analysis of the Si—O bond lengths involved in the Si1—O2—Si2 angle revealed that even though the mean value of 1.66 (3) Å is in good agreement with the expected value, the whole distribution was shifted towards longer, in several cases quite unrealistic, bond lengths. A graphic summary of the Si1—O2—Si2 angles gave a bell-shaped, just slightly right-skewed unimodal distribution with a mean value of 142 (8)°. Finally, the average hexagonal fractional coordinates of Si1, O2 and Si2 were calculated from all the configurations. The x,y coordinates of Si1 [0.00 (1), 0.014 (7)], O2 [0.03 (2), 0.01 (2)] and Si2 [−0.006 (10), −0.002 (8)] atoms correspond to the time-averaged structure with all three atoms on a threefold axis. It is thus evident that X-ray structure analysis itself cannot provide a true picture of the DD-3R structure.

To reveal the possible dynamic disorder in the structure and to analyze the spatial distribution of the atoms during a longer time interval, the MD simulation given in (ii) was carried out. To reveal the basic features hidden in the resulting time series, wavelet denoizing (see *e.g.* Smrčok *et al.*, 1999) and non-decimating wavelet transform (Nason & Von Sachs, 1999; Pichot *et al.*, 1999) were used. It should be stressed that 'denoizing' in this context means removing the high-frequency oscillations and/or random spikes rather than removing the statistical noise. The original and denoized time variations of

the Si1—O2 and Si2—O2 interatomic distances and the Si1—O2—Si2 angle are shown in Fig. 3. The similarity of the time variations of the distances indicate the Si—O—Si bending motion. Correlation between the time variation of the bond distances and the bond angle is better seen from the lowest frequency part of the non-decimating wavelet transforms of the corresponding time series. In Fig. 4 it is shown how a wavelet analysis of such a non-stationary time series (in this case the development of the Si1—O2—Si2 angle in time) allows the evolution of the presence of each frequency contained in the initial signal through time to be followed. The lowest frequency parts of the decompositions of the temporal development of Si1— or Si2—O2 distances and Si1—O2—Si2 angles are compared in Fig. 5. Synchronous changes of both Si—O distances are evident and point to a possible correlated shift – a temporally localized phenomena – of whole building units.

To calculate the frequency of such a Si—O—Si bending vibration, the total (DOS) and partial vibrational density-of-states (PDOS) were calculated from atom velocities. According to Swainson *et al.* (2003), the total calculated spectrum (Fig. 6, inset) can be roughly divided into three parts: vibrational (> 60 meV), lattice and O—Si—O′ bending modes (34–60 meV) and the so-called 'rigid unit modes' (< 34 meV). To understand the dynamic disorder in DD-3*R* zeolite, only the low-energy regions are important, because this kind of disorder cannot significantly change the basic vibrational frequencies. The total contribution of the O2 shift to the spectrum (PDOS) is shown in Fig. 6. The interpretation of the calculated spectra could be based on the INS spectra of various silica polymorphs collected by several authors. For instance, Buchenau *et al.* (1984) analyzed the low-frequency vibrations in vitreous silica in energy gain spectra and proposed that the low-frequency modes originated from

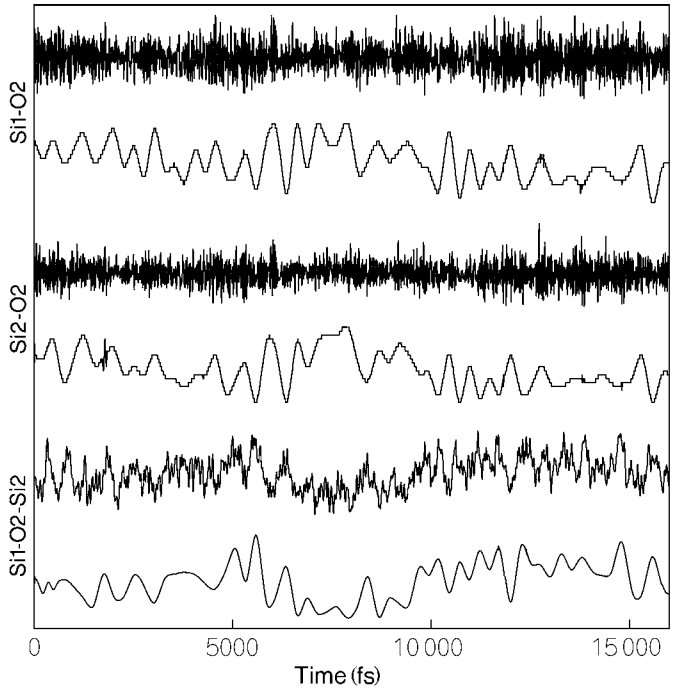

Figure 3
Original and denoized time series showing the variations in Si1—O2 distances (top), Si2—O2 distances (middle) and Si1—O2—Si2 bond angles (bottom). The original amplitudes of bond lenghts (Å) and angles (°) were ⟨1.523;1.716⟩, ⟨1.524;1.767⟩ and ⟨129.2;179.2⟩, respectively.

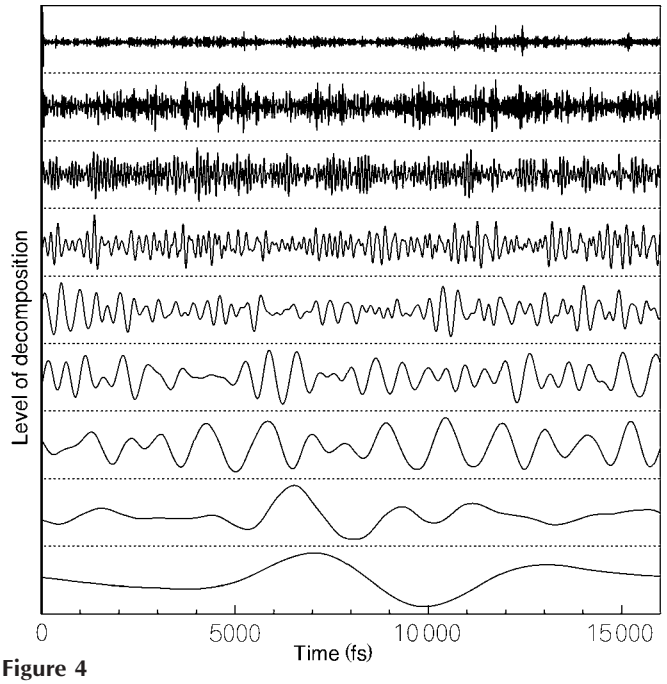

Figure 4
Wavelet decomposition of the signal representing the temporal variation of the Si1—O2—Si2 bond angle. The contributing frequencies are ordered from high (top) to low (bottom). Note that for the sake of clarity the highest frequency component has been omited.

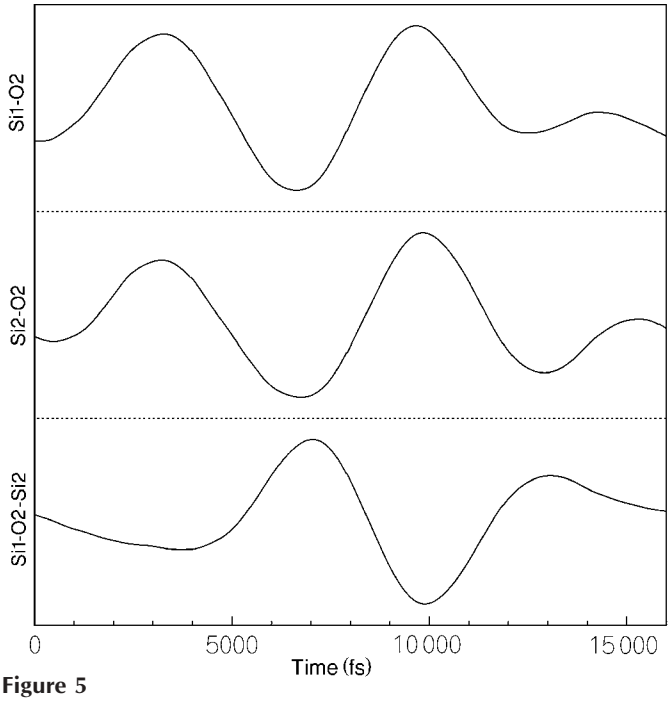

Figure 5
The lowest frequency components of the temporal variation of the Si1—O2 distance (top), the Si2—O2 distance (middle) and the Si1—O2—Si2 bond angle (bottom).

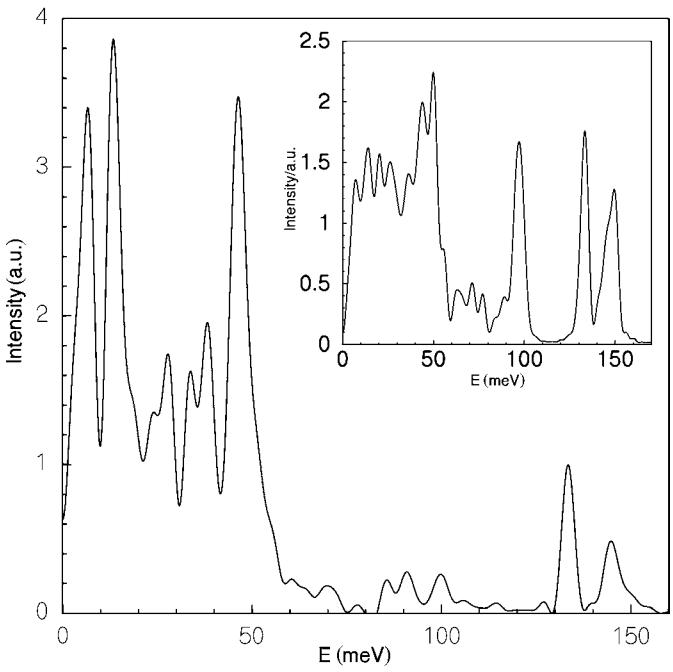

Figure 6
Calculated total (inset) and partial vibrational density-of-states. The low-energy section of the spectra (< 20 meV) shows two peaks, whose positions are comparable to the peak positions found by INS for various silica polymorphs. 1 meV $\simeq$ 8 cm^{-1}.

coupled rotations of the neighbouring SiO_4 tetrahedra, *i.e.* of a rotation of rigid units. In a recent study Nakamura *et al.* (2001) interpreted the modes extending up to 55 meV obtained for vitreous silica, polycrystalline α-cristobalite and α-quartz as stemming from short-range order, *i.e.* from the connectivity of SiO_4 units. The application of the first-principles calculations to a study of the vibrational properties of vitreous SiO_2 was reported by Pasquarello *et al.* (1998). Analyzing PDOS for Si and O they concluded that the peaks at < 70 meV arose mainly from the rocking motions of the O atoms in the direction perpendicular to the Si—O—Si planes.[3]

A comparison of the 0–20 meV part of the PDOS (Fig. 6) with energy transfers obtained for silica polymorphs gives a good correspondence with the experimental spectrum collected for α-quartz. It should be stressed that a full discussion of the dynamic structure of the title compound is not possible without an INS spectrum of DD-3*R*. However, owing to the chemical and structural similarity of silica polymorphs with the title compound, it can be concluded that good agreement of the low-frequency features in the INS spectra with our results from MD indicate that the nature of disorder in DD-3*R* is dynamic rather than static.

One of us (L. S.) is very indebted to Dr Brigitte Bitschnau from the Technical University in Graz for turning his attention to the problem of dodecasil structure. We are grateful for technical support and computer time at the Linux-PC cluster Schrödinger II of the Computer centre of the University of Vienna. We also thank two anonymous referees for constructive criticism of an earlier draft of this paper.

[3] This list of references is far from being complete and a reader requiring more information is kindly asked to refer to *e.g.* Leadbetter (1969), Swainson & Dove (1993), Dove, Harris *et al.* (1997), Harris *et al.* (2000).

References

Almazeestraten, N. C. M., Keysper, J. & Gies, H. (1987). *Z. Kristallogr.* **17**, 6–7.
Baur, W. H. (1977). *Acta Cryst.* B**33,** 2615–2619.
Baur, W. H. (1980). *Acta Cryst.* B**36**, 2198–2202.
Blessing, R. H. (1995). *Acta Cryst.* A**51**, 33–38.
Blöchl, P. E. (1994). *Phys. Rev. B*, **50**, 17953–17979.
Brandenburg, K. (2000). *DIAMOND*, Version 2.1.d. Crystal Impact GbR, Bonn, Germany.
Bruker (2001). *SHELXTL*, Version 6.10. Bruker Axs Inc., Madison, Wisconsin, USA.
Buchenau, U., Nücker, N. & Dianoux, A. J. (1984). *Phys. Rev. Lett.* **53**, 2316–2319.
Demuth, Th., Jeanvoine, Y., Hafner, J. & Ángyán, J. G. (1999). *J. Phys. Condens. Matter*, **11**, 3833–3874.
Dove, M. T., Harris, M. J., Hannon, A. C., Parker, J. M., Swainson, I. P. & Gambhir, M. (1997). *Phys. Rev. Lett.* **78**, 1070–1073.
Dove, M. T., Keen, D. A., Hannon, A. C. & Swainson, I. P. (1997). *Phys. Chem. Miner.* **24**, 311–317.
Ermoshin, V. A., Flachenecker, G., Materny, A. & Engel, V. (1999). *Chem. Phys. Lett.* **311**, 146–152.
Ermoshin, V. A., Flachenecker, G., Materny, A. & Engel, V. (2001). *J. Chem. Phys.* **114**, 8132–8138.
Exter, M. J. den, Jansen, J. C. & van Bekkum, H. (1994). *Zeol. Rel. Micropor. Mater.* **84**, 1159–1166.
Exter, M. J. den, Jansen, J. C., van Bekkum, H. & Zikanova, A. (1997). *Zeolites*, **19**, 353–358.
Ferrario, M. & Ryckaert, J. P. (1985). *Mol. Phys.* **54**, 587–603.
Gambhir, M., Dove, M. T. & Heine, V. (1999). *Phys. Chem. Miner.* **26**, 484–495.
Gies, H. (1986). *Z. Kristallogr.* **175**, 93–104.
Gies, H. & Czank, M. Z. (1986). *Z. Kristallogr.* **174**, 64–65.
Goor, G. van de (1995). PhD Thesis. University of Konstanz, Germany.
Harris, M. J., Dove, M. T. & Parker, J. M. (2000). *Mineral. Mag.* **64**, 435–440.
Hatop, H., Schiefer, M., Roesky, H. W., Herbst-Irmer, R. & Labahn, T. (2001). *Organometallics*, **20**, 2643–2646.
Herbst-Irmer, R. & Sheldrick, G. M. (1998). *Acta Cryst.* B**54**, 443–449.
Herbst-Irmer, R. & Sheldrick, G. M. (2002). *Acta Cryst.* B**58**, 477–481.
Könnecke, M., Miehe, G. & Fuess, H. (1992). *Z. Kristallogr.* **201**, 147–155.
Knorr, K. & Depmeier, W. (1997). *Acta Cryst.* B**53**, 18–24.
Kresse, G. & Furthmüller, (1996). *J. Comput. Mater. Sci.* **6**, 15–50.
Kresse, G. & Hafner, J. (1993). *Phys. Rev. B*, **48**, 13115–13118.
Kresse, G. & Hafner, J. (1994). *J. Phys. Condens. Matter* **6**, 8245–8527.
Kresse, G. & Joubert, D. (1999). *Phys. Rev. B*, **59**, 1758–1775.
Leadbetter, A. J. (1969). *J. Chem. Phys.* **51**, 779–786.
Miehe, G., Vogt, T. & Fuess, H. (1993). *Acta Cryst.* B**49**, 745–754.
Nason, G. P. & Von Sachs, R. (1999). *Philos. Trans. R. Soc. London A*, **357**, 2511–2526.
Nakamura, M., Arai, M., Otomo, T., Inamura, Y. & Bennington, S. M. (2001). *J. Non-Cryst. Solids*, **293–295**, 377–382.
Nespolo, M. (2004). *Z. Kristallogr.* **219**, 57–71.
Nosé, S. (1984). *J. Chem. Phys.* **81**, 511–519.
Pasquarello, A., Sarnthein, J. & Carr, R. (1998). *Phys. Rev. B*, **57**, 14133–14139.
Peacor, D. R. (1973). *Z. Kristallogr.* **138**, 274–298.
Perdew, J. P. & Zunger, A. (1981). *Phys. Rev. B*, **23**, 5048–5079.
Perdew, J. P. & Wang, Y. (1992). *Phys. Rev. B*, **45**, 13244–13249.

Pichot, V., Gaspzo, J.-M., Molliex, S., Antoniadis, A., Busso, T., Roche, F., Costes, F., Quintin, L., Lacour, J.-R. & Barthélémy, J.-C. (1999). *J. Appl. Physiol.* **83**, 1081–1091.
Schmahl, W. W., Swainson, I. P., Dove, M. T. & Graeme-Barber, A. (1992). *Z. Kristallogr.* **201**, 125–145.
Sheldrick, G. M. (2001). *SADABS*. University of Göttingen, Germany.
Siemens (1995). *SMART, SAINT* and *XPREP*. Siemens Analytical X-ray Instruments Inc., Madison, Wisconsin, USA.
Smrčok, Ľ., Ďurík, M. & Jorik, V. (1999). *Powder Diffr.* **14**, 300–304.
Swainson, I. P. & Dove, M. T. (1993). *Phys. Rev. Lett.* **71**, 193–196.
Swainson, I. P., Dove, M. T. & Palmer, D. C. (2003). *Phys. Chem. Miner.* **30**, 353–365.
Tucker, M. G., Squires, M. P., Dove, M. T. & Keen, D. A. (2001). *J. Phys. Condens. Matter*, **13**, 403–423.
Wilson, A. J. C. (1985). Editor. *Structure and Statistics in Crystallography*. Guilderland, NY: Adenine Press.
Wirnsberger, G., Fritzer, H. P., van de Goor, G., Pillep, B., Behrens, P. & Popitsch, A. (1997). *J. Mol. Struct.* **410**, 123–127.
Wirnsberger, G., Fritzer, H. P., Koller, H., Behrens, P. & Popitsch, A. (1999). *J. Mol. Struct.* **481**, 699–704.